Cui et al. Cell Communication and Signaling (2024) 22:560
https://doi.org/10.1186/s12964-024-01927-w

Cell Communication and Signaling

RESEARCH Open Access

Exploiting potential molecular compounds for treating testicular seminoma by targeting immune related genes

Yankang Cui[1†], Xiaodie Zhou[2†], Jing Zhang[3†], Bo Fang[1], Jingping Ge[1], Hao Tang[1], Bianjiang Liu[4], Haowei He[1*], Feng Xu[1*] and Xuejun Shang[1*]

Abstract

Background In cases of advanced seminoma, up to 30% of patients may manifest cisplatin resistance, necessitating aggressive salvage therapy, with a consequent 50% risk of mortality attributable to cancer. Nevertheless, beyond chemotherapy and radiotherapy, no further therapeutic modalities have been implemented for these patients.

Methods The study commenced with the identification of differentially expressed immune-related genes, which were subsequently subjected to clustering using WGCNA. Prognostic signature construction ensued through the execution of univariable Cox regression, lasso regression, and multivariable Cox regression analyses. To validate the prognostic signature, the TCGA-TGCT and GSE99420 cohorts were employed, with assessments conducted via PFS, C-index, DCA, and ROC analyses. Subsequent exploration of the immune landscape and potential immunotherapeutic applications was undertaken through Cibersort and TIDE analyses. Molecular docking and dynamics simulation techniques were then employed for screening potential molecular compounds. Validation of these findings was pursued through in vitro and vivo assays.

Results CTLA4, SNX17, and TMX1 were selected to construct the signature. Patients in the high-risk group exhibited diminished progression-free survival rates. The AUC for predicting survival at 1, 3, and 5 years was 0.802, 0.899, and 0.943, respectively, surpassing those of other risk factors, such as lymphovascular invasion and T stage. The C-index for the risk score was 0.838. Decision curve analysis (DCA) suggests that incorporating lymphovascular invasion and the risk score yields the most favorable decision-making outcomes for patients. Moreover, individuals classified as high-risk may derive greater benefit from immunotherapy. Molecular compounds including Rutin, ICG-001, and Doxorubicin can selectively target CTLA4, SNX17, and TMX1, respectively, thereby inhibiting the proliferation and invasive capabilities of seminoma tumor cells in vitro and vivo.

†Yankang Cui, Jing Zhang and Xiaodie Zhou contributed equally to this work.

*Correspondence:
Haowei He
hehaowei1982@hotmail.com
Feng Xu
msn1999@sina.com
Xuejun Shang
shangxj98@sina.com

Full list of author information is available at the end of the article

Conclusion The signature initially constructed based on immune-related genes shows promise for predicting outcomes and assessing the efficacy of immunotherapy in seminoma patients. Rutin, ICG-001, and Doxorubicin have demonstrated potential to target these signature genes and inhibit tumor cell viability.

Keywords Seminoma, Signature, Immune related genes, Prognosis, Molecular compounds

Graphical Abstract

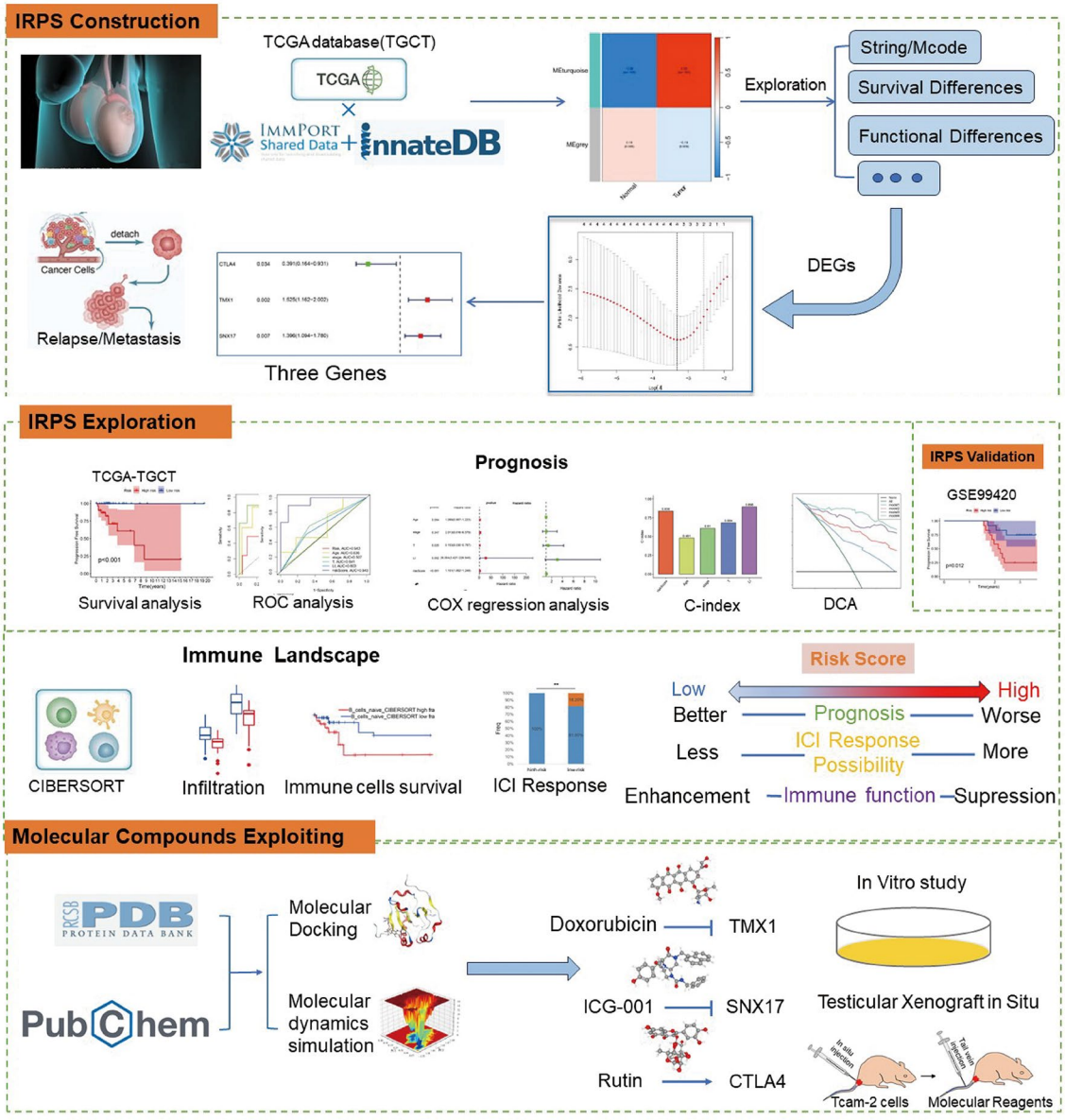

Introduction

Testicular germ cell tumors (TGCTs) are acknowledged as one of the most prevalent urological malignancies, exhibiting a paradoxical trend of increasing incidence despite their relatively low prevalence [1]. Moreover, they represent the predominant solid tumor type among young men aged 15–34, with approximately 50% of cases characterized by seminomatous histology [2]. Projections for 2023 in the United States alone anticipate 9190 new diagnoses and 470 fatalities, primarily attributed to tumor metastasis, recurrence, or chemotherapy resistance [3]. Remarkably, at the time of TGCT diagnosis, an estimated 32.2% of patients have already experienced metastasis, with 25% of this subset destined for tumor recurrence [4]. Findings from an investigation focused on stage I testicular tumors indicate that 18.9%

of patients endure tumor recurrence, with nearly half of these relapsed cases necessitating additional chemotherapy or radiotherapy due to metastatic spread or relapse, thus presenting formidable challenges for chemoresistant patients seeking benefits from established therapeutic modalities [5]. Furthermore, the heightened invasiveness of testicular tumor cells serves as a significant prognostic indicator for tumor recurrence and unfavorable clinical outcomes [6].

A nationwide, population-based cohort study conducted in Denmark, involving 924 patients, disclosed that 148 (16%) patients experienced relapse during a median follow-up period of 6.3 years. Factors including invasion of the testicular hilum (including rete testis and hilar soft tissue), lymphovascular invasion, and elevated pre-orchiectomy levels of β-human chorionic gonadotropin (β-HCG) and lactate dehydrogenase (LDH) emerged as independent predictors of relapse [7]. As illustrated in Table 1, a study encompassing advanced germ cell tumors revealed that all seminoma patients experiencing progression were resistant to chemotherapy [8]. These findings emphasize the necessity to explore additional treatment strategies for advanced seminoma patients.

The clinical efficacy of checkpoint inhibitors targeting the PD-1/PD-L1 system is remarkable across various cancers [9, 10], with prior investigations indicating a prognostic significance of PD-L1-expressing tumor-infiltrating lymphocytes in seminoma specimens [11, 12]. Furthermore, there is considerable optimism regarding the potential of combinatorial drug approaches targeting multiple immune checkpoint receptors to improve therapeutic outcomes. In the present study, we have developed a prognostic signature based on immune-related genes. Subsequent validation and analyses have demonstrated that this signature reliably predicts outcomes and sensitivity to immunotherapies (ICI). Additionally, we have identified three small molecule inhibitors or agonists capable of modulating the expression of these signature genes. In summary, this study represents the first attempt to construct an immune-related signature for predicting disease progression and responsiveness to immunotherapy in seminoma patients. Further experimental investigations hold promise for advancing our understanding of

Table 1 The correlation between clinical characteristics and cisplatin sensitivity

Characteristic	No%		*P* value
	Cisplatin resistance(*N* = 24)	Cisplatin sensitivity(*N* = 21)	
Age			1
<=35	8(33.33%)	7(33.33%)	
> 35	16(66.67%)	14(66.67%)	
Progression of Disease			**0***
No	0(0%)	21(100%)	
Yes	24(100%)	0(0%)	
Igcccg stage			0.6328
1	19(79.17%)	17(80.95%)	
2	4(16.67%)	4(19.05%)	
3	1(4.17%)	0(0%)	
S Stage			**0.0143***
S0	11(45.83%)	14(66.67%)	
S1	3(12.5%)	3(14.29%)	
S2	10(41.67%)	1(4.76%)	
S3	0(0%)	3(14.29%)	
M Stage			1
M0	19(79.17%)	16(76.19%)	
M1	5(20.83%)	5(23.81%)	
N Stage			0.0967
N0	4(16.67%)	9(42.86%)	
N1	2(8.33%)	4(19.05%)	
N2	3(12.5%)	1(4.76%)	
N3	15(62.5%)	7(33.33%)	
T			0.261
T0	1(4.17%)	0(0%)	
T1	11(45.83%)	15(71.43%)	
T2	10(41.67%)	4(19.05%)	
T3	2(8.33%)	2(9.52%)	

seminoma pathogenesis and facilitating the development of novel immunotherapeutic approaches.

Materials and methods

Data collection and pre-processing

Transcriptome profiling data (Count) of TGCT was downloaded from the Cancer Genome Atlas (TCGA, https://portal.gdc.cancer.gov/). Seminoma samples were included and divided into relapse (R) and non-relapse (NR) groups after reviewing the clinical data. The RNA-seq data and clinical information of the independent external validation cohort (GSE99420) was obtained from the Gene Expression Omnibus (GEO, https://www.ncbi.nlm.nih.gov/geo/) dataset. Single cell RNA-seq (scRNA-seq, GSE197778) data was also downloaded from the GEO dataset. Normal testis samples were obtained from the Genotype-Tissue Expression (GTEx, www.gtexportal.org/) dataset. Clinical data of chemical response was obtained from the Cbioportal dataset (MSK, J Clin Oncol 2016) [8]. The raw datasets, after calibration and normalization, were all converted to log2 forma using algorithm in R.

Identification of immune-related hub genes

The immune-related gene lists were obtained from ImmPort and InnateDB databases. After standardization of the expression matrix using "normalizeBetweenArrays" package in R, the differential expression immune related genes (IRGs) between seminoma and normal testis were explored with "limma" package and displayed with "pheatmap" package. $|\mathrm{Log_2Fold\ change\ (FC)}| > 2$ and p-value < 0.01 were set as the criteria for identifying differentially expressed IRGs.

Weighted Gene Co-expression Network (WGCNA) was then performed using the "WGCNA" package in R. First, the mean expression of each gene (meanFPKM) was determined, and the genes with meanFPKM < 0.5 were removed. Second, the gene expression matrix was filtered by the "goodSamplesGenes" function to check missing values. Third, adjacency was computed using the "soft" thresholding power. The adjacency was then converted into a topological overlap matrix (TOM). The gene ratio and dissimilarity were determined subsequently. Afterward, the hierarchical clustering and dynamic tree cut functions were used to detect the modules. With a minimum gene group size ($n = 50$) and a TOM-based dissimilarity metric, genes with identical expression profiles were classified into gene modules using average linkage hierarchical clustering. Finally, the dissimilarity of module eigengenes was computed, a cut line for the module dendrogram was chosen, and several modules were combined for further investigation.

The String dataset (https://cn.string-db.org/) was used to visualize the network between the most significant module genes, and the Molecular Complex Detection (mcode), a plugin for Cytoscape (V3.9.0), was applied to construct the key-clusters in the network. The criteria for selection were set as follows: degree cut-off = 2, maximum depth = 100, node score cut-off = 0.2, and K-score = 2. The genes in the key cluster were considered as hub-genes.

We performed Gene set enrichment analyses (GSEA) to define the hub-genes in the Gene Ontology (GO) and Kyoto Encyclopedia of Genes and Genomes (KEGG) respectively. Statistical significance was set at $P < 0.05$ and false discovery rate (FDR) $q < 0.05$. The procedure was performed using R packages including "clusterProfiler", "org.Hs.eg.db", "circlize", and "dplyr".

Immune-related Prognostic signature (IRPS) construction and validation

All of the hub-genes were performed with progression free survival (PFS) analysis, and the survival related genes were deemed eligible for model construction. We conducted univariable COX proportional hazards regression analysis, lasso regression and multivariable COX regression analysis in order to construct the prognostic model. The p value filter for univariable COX regression was 0.05 and significant genes were further enrolled to conduct lasso regression. The Akaike information criterion (AIC) values were used to optimize the multivariable COX model and the RNAs with the lowest AIC were retained in the final signature. The risk score formula was as followed: Risk score= $\sum$Gene(exp)×Gene(coef) (Gene(exp) indicates the expression of every single RNA and the Gene(coef) was calculated using a multivariable COX proportional hazards model). Samples were defined as high-risk samples or low-risk samples based on the median risk score. The differential expression analyses of the immune-related signature genes (IRSGs) between seminoma and normal testis, R and NR were performed with "limma" package.

Kaplan-Meier curve and log-rank test were conducted to evaluate the relationship between PFS and risk score, based on TCGA-TGCT dataset and external validation cohort GSE99420 dataset.

Univariable and multivariable COX regression analyses were performed to assess the risk factors of age, stage, T, Lymphovascular Invasion (LI) and risk score in seminoma patients. The ROC analyses were subsequently performed to assess the signature's prognostic value based on PFS years and risk factors (age, stage, T, LI, and risk score). Concordance index (C-index) was calculated with "dplyr", "rms" and "pec" packages in R software. "Regplot", "rms" and "survival" packages were used to establish the nomogram. "ggDCA" package was used to perform the Decision Curve Analysis (DCA). Principal components analysis (PCA) was performed based on TCGA-TGCT

and GSE99429 datasets respectively using the R "scatterplot3d" package.

CIBERSORT and immune therapy response

CIBERSORT was used to assess the infiltration pattern of 22 tumor immune cells in seminoma patients. The difference of immune cells infiltrating level between high and low risk groups was compared with Wilcoxon rank-sum test. For correlation test between IRSGs and the infiltration of immune cells, Spearman test was utilized. The differences between high and low risk groups in immune functions were performed with "GSVA" package. Furthermore, the tumor immune dysfunction and exclusion (TIDE) tool (http://tide.dfci.harvard.edu/) from the Harv ard University was used to assess the clinical efficiency of immune checkpoint inhibition therapy. The higher TIDE predictive scores correlate with poor therapeutic effect and worse prognosis.

scRNA-seq analysis

We performed an analysis of single-cell RNA sequencing (scRNA-seq) data using R packages, including "Seurat" and "SingleR". To ensure high-quality data, three filtering criteria were applied to each cell: (1) genes expressed in at least 5 single cells were retained, (2) cells with more than 5% mitochondrial genes were excluded, and (3) cells expressing fewer than 100 genes were removed. Initially, the scRNA-seq data underwent normalization using the "LogNormalize" method. The normalized data were then transformed into a Seurat object, and the top 1,500 highly variable genes were identified using the "FindVariableFeatures" function. Subsequently, the "RunPCA" function from the "Seurat" R package was employed to conduct principal component analysis (PCA), reducing the dimensionality of the scRNA-seq data based on the top 1,500 genes. Significant principal components were identified using JackStraw analysis, and the first 15 principal components, selected based on the proportion of variance explained, were utilized for cell clustering. Cell clustering analysis was performed using the "FindNeighbors" and "FindClusters" functions within the "Seurat" package. A k-nearest neighbor graph was constructed based on Euclidean distance in PCA, with the "FindNeighbors" function determining the closest neighbors of each cell. Subsequently, t-distributed stochastic neighbor embedding (t-SNE) was conducted using the "RunTSNE" function to visualize cell clustering, represented in t-SNE-1 and t-SNE-2 dimensions. Differential expression analysis was carried out using the "FindAllMarkers" function within the "Seurat" package, employing Wilcoxon–Mann–Whitney tests to identify differentially expressed genes (DEGs) for each cluster. Marker genes for each cluster were determined based on cutoff threshold values, with an adjusted p-value < 0.01 and |log2 (fold change)| >1. For cluster annotation, a reference-based annotation approach was employed, utilizing reference data from the Human Primary Cell Atlas.

Sample collection

Seminoma samples and adjacent normal tissues were obtained from 38 patients (mean age: 34±4 years, range: 21–43 years) between 2011 and 2021 at the First Affiliated Hospital of Nanjing Medical University and Nanjing Jinling Hospital. These patients underwent orchiectomy and were subsequently diagnosed with testicular seminoma based on postoperative pathology. Among them 12 patients suffered relapse after surgery (7 of them locoregional recurrence; 4 of them new primary tumor, 1 of them distant metastasis). Samples for RNA extraction were promptly frozen in liquid nitrogen and stored at -80 °C. Samples intended for immunohistochemical analysis were fixed in formalin. The study design and protocol were ethically approved by the ethics committee of the Jinling Hospital, and informed consent was obtained from all participants.

RNA extraction, reverse transcription, and quantitative RT-PCR

Total RNA was extracted from testis tissues and cell lines using TRIzol reagent (Invitrogen, Carlsbad, CA, USA). The total RNA was reverse-transcribed into complementary DNA (cDNA) using HiScript II (Vazyme, Shanghai, China). qRT-PCR was performed using SYBR Green I (Vazyme, Shanghai, China) on ABI 7900 system (Applied Biosystems, Carlsbad, CA, USA) and the primers were as followed: CTLA4 Forward: 5'-GCCCTGCACTCTCCTG TTTTT-3'; CTLA4 Reverse: 5'-GGTTGCCGCACAGAC TTCA-3'. SNX17 Forward: 5'- CGCCTACGTGGCCTAT AACAT-3'; SNX17 Reverse: 5'- CAATGGGTCTTGCCG AACAG-3'. TMX1 Forward: 5'- TTGCGAAAGTAGATG TCACAGAG-3'; TMX1 Reverse: 5'- CTGATAGCGCCT AAATTCACCAT-3'; β-actin Forward, GAAGATCAAG ATCATTGCTCCT; β-actin Reverse, TACTCCTGCTTG CTGATCCA).

Immunohistochemistry (IHC) and immunofluorescence (IF)

IHC staining and evaluation followed previously established protocols [19]. Specifically, protein expression levels of CTLA4, SNX17, and TMX1 in both seminoma and adjacent normal testis tissues were assessed using anti-CTLA4, anti-SNX17, and anti-TMX1 antibodies, respectively.

For tissues representing both relapse and non-relapse seminomas, coverslips were initially washed three times in PBS, followed by fixation in 4% paraformaldehyde for 15 min. Subsequently, permeabilization was achieved by treating slides with 0.5% Triton X-100 at room temperature for 20 min, followed by three PBS washes and

blocking with 2% BSA for 30 min. Slides were then incubated overnight at 4 °C with the appropriate primary antibodies (Concentration: CTLA4-1:1000; TMX1-1:1000; SNX17-1:1000; CD27-1:1000; CD22-1:3000; CD3-1:3000; VIMENTIN-1:5000), followed by incubation with secondary antibodies (1:300) at room temperature for 2 h. Nuclei were counterstained with DAPI, and the slides were scanned using a 3DHISTECH scanner (Pannoramic MIDI). For the analysis of immunofluorescence staining intensity, we utilized ImageJ software to calculate the intensities of DAPI and the markers. The relative immunofluorescence intensity was calculated using the following formula: relative immunofluorescence intensity=intensity of marker / intensity of DAPI.

Cell culture

The Tcam-2 cell line, derived from testicular seminoma, was procured from the Department of Urology, Sir Run Run Shaw Hospital, Zhejiang University School of Medicine. The cells were cultured in DMEM medium (Gibco, Grand Island, NY) supplemented with 10% fetal bovine serum (FBS) (Gibco, Grand Island, NY) at 37 °C in a 5% CO_2 atmosphere.

Antibodies and reagents

Primary antibodies were obtained from: Mouse anti-CTLA4 (Santa Cruz, sc-376016), Rabbit anti-SNX17 (abcam, ab223046), Rabbit anti-TMX1 (abcam, ab244263), anti-GAPDH, CD27, CD22, CD3, Vimentin, E-cad, N-cad, Ki-67 were all obtained from Servicebio technology. Secondary antibodies including anti-mouse IgG, anti-rabbit IgG, Alexa Fluor Secondary antibody (Spectrum 440- aqua, 488-green, 546-red, 594-orange, 647-yellow) were also gained from Servicebio technology. Rutin, ICG-001, and Doxorubicin were obtained from Selleck chem.

Cell proliferation assay and colony formation assay

To assess cellular proliferation, Tcam-2 cells were seeded at a density of 2×10^3 cells per well in 96-well plates. The CCK-8 system (Dojindo, Japan) was subsequently added to each well at 0, 1, 2, 3, and 4 days of culture following the manufacturer's instructions. Absorbance readings at 450 nm were taken using a microplate reader (Tecan, Switzerland) to determine cell viability.

For the colony formation assay, approximately 1×10^3 cells were plated in six-well dishes and treated with DMSO, Rutin, ICG-001, and Doxorubicin, respectively. After two weeks of incubation, colonies were fixed with paraformaldehyde, stained with 0.1% crystal violet, and subsequently imaged and counted.

Wound healing and transwell assay

Cells were seeded into six-well plates at a density of 3×10^5 cells per well and cultured until reaching 90–100% confluence. Following scratching with a 10-uL pipette tip, wells were washed twice with PBS to eliminate cell debris and residual serum. Subsequently, cells were cultured in serum-free DMEM for an additional 12 h. The wound edges were photographed using DP-BSW software (10× objective) 12 h post-injury and measured using ImageJ software.

For transwell assays, cells were seeded at a density of 1×10^5 cells in 200 μL of serum-free medium onto the upper chamber with an 8-mm pore size, either coated or uncoated with 50 μL of Matrigel (BD Biosciences). The lower chambers were filled with DMEM containing 20% FBS as a chemoattractant. Following incubation at 37 °C for 12 h for migration and 48 h for invasion, cells that had migrated to the underside of the membrane were fixed in 4% paraformaldehyde for 30 min and subsequently stained with 2% crystal violet. Non-migrating or non-invading cells were gently removed, and cells that had migrated to the outer chamber were counted in five representative fields at 200× magnification.

Western blotting

Cells treated with reagents were lysed using radioimmunoprecipitation assay (RIPA) lysis buffer (Beyotime Biotechnology, Shanghai, China). The harvested proteins were quantified using the bicinchoninic acid (BCA) kit (Beyotime Biotechnology), separated on a 10% sodium dodecyl sulfate polyacrylamide gel electrophoresis (SDS-PAGE), and transferred onto polyvinylidene fluoride (PVDF) membranes (Sigma-Aldrich, St. Louis, MO). These membranes were then blocked in Tris-buffered saline (TBS) containing 5% non-fat milk for 2 h. Following overnight incubation with primary antibodies at 4 °C (Concentration: CTLA4 1: 1500; TMX1 1:1000; SNX17 1:1000; E-cad 1:2000; N-cad 1:1500; Vimentin 1:1000), the membranes underwent three washes with TBS containing 0.1% Tween 20 (TBST). Subsequently, they were incubated with secondary antibody solution (1:1000) at room temperature for 2 h. Following another round of washing, the signals were detected using a chemiluminescence system and analyzed with Image Lab software.

Xenografts in mice

For testicular xenografts in situ, 2×10^8 of Tcam-2 cells were harvested and mixed with Matrigel in a 1:1 ratio. The cell mixture was then injected into the testes of male nude mice aged 4–6 weeks, with five mice per group and a total of four groups. DMSO, Rutin, ICG-001, and Doxorubicin were administered intravenously via the tail vein once a week. After five weeks, the mice were euthanized, and the tumor masses were promptly excised for

immediate measurement of weight and volume. Tumor dimensions (length L and width W) were recorded to calculate tumor volume (V) using the formula: V = (L * W^2) / 2.

Molecular compound screening and docking

The protein crystal structures of the three IRSGs were downloaded from the PDB dataset. The candidate molecular structures were downloaded from the Pubchem dataset (Table S1). The Molecular Operating Environment (MOE) software (version 2019.0102) was utilized to prepare protein structures and conduct docking scoring. In brief, the active site was determined for each enzyme using the MOE alpha site finder. Ligand molecules were then positioned within the site using the Triangle Matcher method and ranked utilizing the London dG scoring function. Subsequently, the ten best poses (with a default of 30) were selected and subjected to further refinement through energy minimization within the binding pocket. Following refinement, rescoring was performed using the GBVI/WSA dG scoring function.

Molecular dynamics simulation

The molecular dynamics simulations utilized Gromacs 2022.3 software [13]. Initial preprocessing of small molecules involved the application of AmberTools22 to apply the GAFF force field and Gaussian 16 W for hydrogenation and calculation of RESP potential. Subsequently, the resulting potential data were integrated into the topology file of the molecular dynamics system. Simulations were conducted under standard conditions, maintaining a static temperature of 300 K and atmospheric pressure (1 bar). The Amber99sb-ildn force field was employed, with water molecules serving as the solvent (Tip3p water model), and the overall charge of the simulation system was neutralized by the addition of an appropriate quantity of Na+ions. The energy minimization stage utilized the steepest descent method, followed by equilibration in the isothermal isovolumetric ensemble (NVT) and isothermal isobaric ensemble (NPT), each for 100,000 steps, with a coupling constant of 0.1 ps and a duration of 100 ps. Subsequently, free molecular dynamics simulations were conducted, spanning 5,000,000 steps with a step length of 2 fs, resulting in a total duration of 100 ns. Post-simulation analysis involved the utilization of the built-in tools within the software to compute various parameters including root-mean-square deviation (RMSD), root-mean-square fluctuation (RMSF), and the protein rotation radius for each amino acid trajectory. Additionally, free energy calculations, such as MMGBSA, and free energy topography were performed, integrating the trajectory data with other pertinent analyses.

Statistical analysis

The majority of analyses were conducted utilizing R software (version 4.0.0) or Perl scripts (version 5.32.0). Perl scripts were primarily employed for data processing tasks, including gene ID transformation and data merging. Group comparisons were conducted using the Student's t-test or chi-square test, as appropriate for the comparison of two or three groups. A significance threshold of $p<0.05$ was applied, unless specified otherwise.

Results

Immune-related hub genes

In the differential expression analysis comparing 66 seminoma samples to 165 normal testes, a total of 766 differentially expressed immune-related genes (IRGs) were identified, with 511 upregulated and 255 downregulated in seminoma compared to normal testes (Fig. 1a and b, Table S2). To identify immune-related hub genes, WGCNA analysis was performed on the candidate genes ($n=766$). A strong positive correlation (scale R^2=0.95) was observed between the logarithm of node connectivity (log(k)) and the logarithm of node probability (log(P(k))) (Figure S1). Two distinct modules were delineated through average linkage hierarchical clustering and optimal soft-thresholding power determination (Fig. 1c). The turquoise module exhibited a high correlation with seminoma (cor=0.96, $P<1e-200$), and genes with module membership (MM) values>0.5 or <-0.5 within the turquoise module were selected for further analysis. Subsequently, a total of 690 module genes were input into the STRING database to construct a Protein-Protein Interaction (PPI) network (Fig. 1e). The network was visualized and analyzed using the MCODE plugin in Cytoscape, revealing a significant cluster with a MCODE score of 31.947, comprising 39 nodes and 1214 edges (Fig. 1f). Gene Ontology (GO) analysis based on these 39 key cluster genes indicated enrichment in the "Cytokine-mediated signaling pathway" and "external side of plasma membrane" (Fig. 1g). Moreover, the "Cytokine-cytokine receptor interaction" pathway emerged as the most significant pathway according to KEGG analysis, positioned centrally within the pathway network (Fig. 1h).

IRPS construction and expression validation

To identify independent prognostic genes, progression-free survival (PFS) analyses were conducted among the 39 immune-related hub genes to assess their association with survival. Subsequently, univariable Cox regression analysis was performed on these survival-related genes, and four genes (CTLA4, SNX17, TMX1, and TBX21) were selected for least absolute shrinkage and selection operator (LASSO) regression analysis (Fig. 2a). Following evaluation based on the Akaike information criterion (AIC) values (Fig. 2b), these four

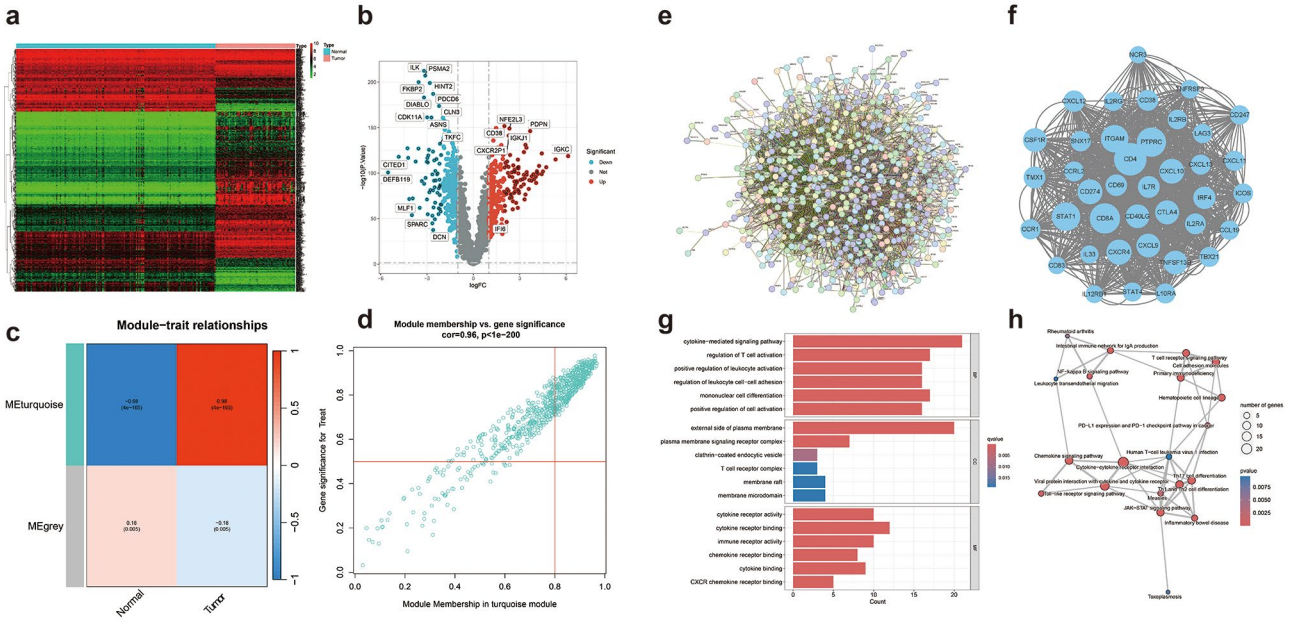

Fig. 1 Immune-related hub genes identified. Heatmap (**a**) and volcano plot (**b**) of differentially expressed genes in TCGA between seminoma and normal testes tissues; (**c**) WGCNA showing significant correlation between module eigengenes and tissues. (**d**) A scatterplot of gene significance versus module membership in the most significant module (turquoise module), with a correlation coefficient of 0.96 and $P < 1e{-}200$. (**e**) The PPI network built by the STRING database basing on 690 module genes. (**f**) The key cluster enriched by Cytoscape software. The GO (**g**) and KEGG (**h**) enrichment of the key cluster genes

genes underwent multivariable Cox regression analysis. Ultimately, CTLA4, SNX17, and TMX1 were utilized to construct the immune-related prognostic signature (IRPS) using the formula: expression level of CTLA4*(-0.66)+expression level of SNX17*0.33+expression level of TMX1*0.37. These three signature genes were found to be upregulated in seminoma tissues compared to normal testes. However, while CTLA4 was downregulated in relapse (R) samples, TMX1 and SNX17 were upregulated in relapse samples relative to non-relapse (NR) samples (Fig. 2d). Notably, higher expression levels of TMX1 and SNX17 were associated with increased risk of relapse (Fig. 2c), categorizing them as risk genes. Conversely, CTLA4 was identified as a protective gene.

To validate the expression pattern of the three signature genes, quantitative real-time polymerase chain reaction (qRT-PCR) analyses were performed on 38 seminoma samples and their corresponding adjacent normal tissues. In accordance with the aforementioned analyses, all three signature genes were found to be upregulated in seminoma samples (Fig. 2e). Additionally, TMX1 and SNX17 exhibited upregulation in relapse samples, while CTLA4 showed downregulation in relapse samples (Fig. 2f). Immunohistochemical (IHC) protein staining corroborated these findings, demonstrating consistent results with mRNA expression (Fig. 2g).

The prognostic validation of IRPS

The samples were stratified into high and low-risk groups based on the IRPS risk score. Patients in the low-risk group exhibited superior PFS compared to those in the high-risk group, evident in both the TCGA-TGCT cohort (Fig. 3a, $P<0.001$) and the validation GSE99420 cohort (Fig. 3b, $P=0.012$). Moreover, as the risk score increased, a higher incidence of relapse and shorter progression survival times were observed, as depicted in Fig. 3c and d. The expression patterns of the three signature genes in the high-risk and low-risk groups are illustrated in the heatmap. Principal component analysis (PCA) scatter plots demonstrated the effective discrimination of samples by the IRPS (Fig. 3e). Furthermore, gene set variation analysis (GSVA) revealed significant enrichment of the "CYTOKINE_CYTOKINE_RECEPTOR_INTERACTION" pathway in the low-risk group and the "MISMATCH_REPAIR" pathway in the high-risk group (Fig. 3f). Missense mutation of KIT and KRAS was existed in both high and low-risk groups (Figure S2).

The AUC values of the IRPS for 1-, 3-, and 5-year survival rates were 0.802, 0.899, and 0.943, respectively (Fig. 4a). In contrast to age (AUC=0.636), stage (AUC=0.507), T (AUC=0.641), and LI (AUC=0.603), the risk score exhibited a higher AUC value of 0.943 (Fig. 4b). Univariable Cox regression analysis indicated that the risk score was an independent risk factor for seminoma patients ($p=0.008$, HR=1.063, 95% CI=1.016–1.112). However, LI was also identified as a risk factor based

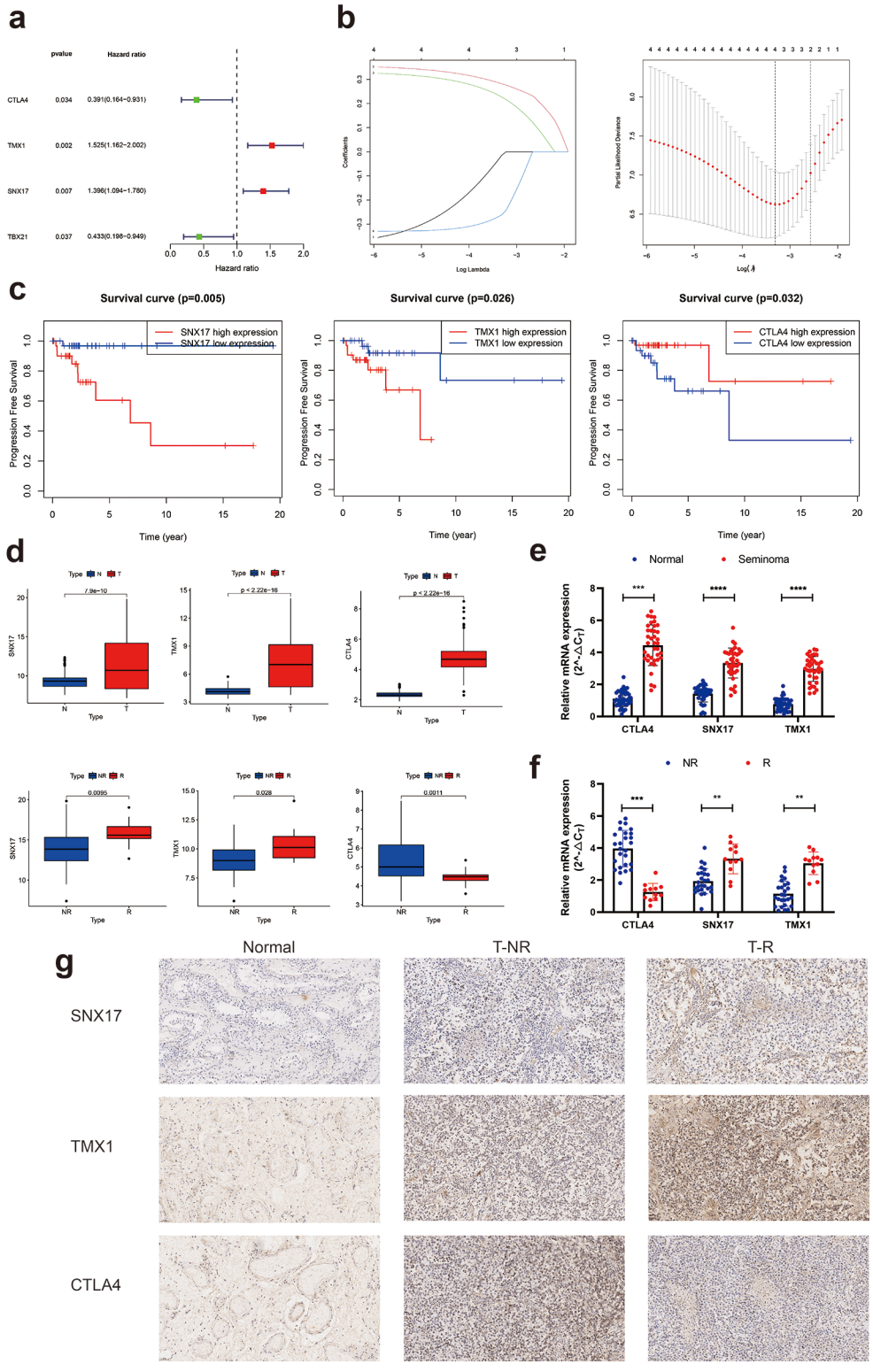

Fig. 2 The construction of IRPS. (**a**) Univariable Cox and Lasso regression analyses (**b**) based on survival-related hub genes. (**c**) The progression free survival analyses of the 3 signature genes. (**d**) The expression pattern of the 3 signature genes. (**e-f**) The validation of mRNA expression and protein expression (**g**) with clinical samples. (R: Relapse; NR: non-relapse; **, $p < 0.01$; ***, $p < 0.001$; ****, $p < 0.0001$)

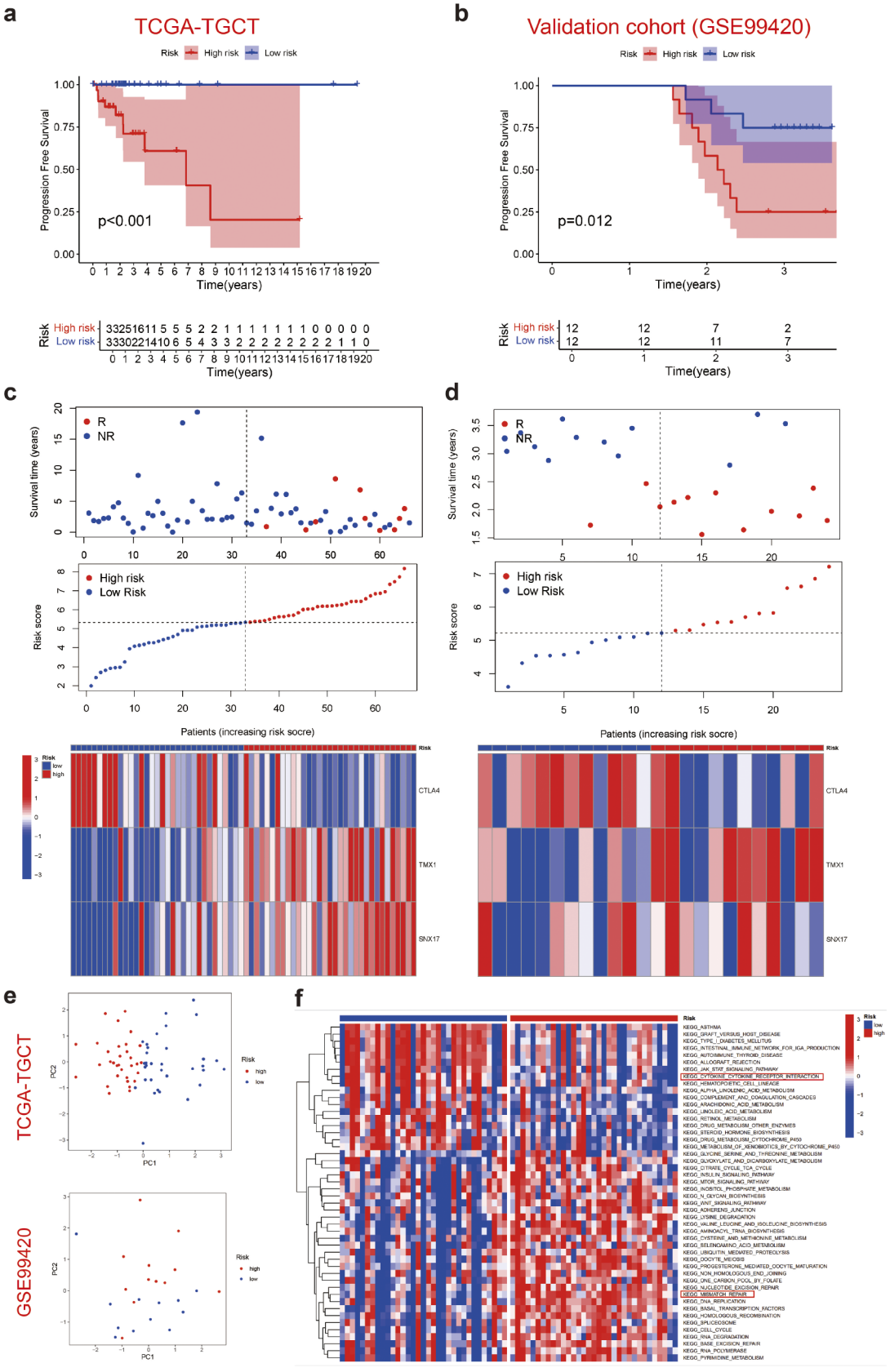

Fig. 3 The validation of IRPS. (**a**) The progression survival analysis based on TCGA and GSE99420 (**b**) seminoma cohorts. (**c-d**) Risk score, distribution of survival status between the high-risk and low-risk groups, and expression heat maps of 3 IRSGs. (**e**) The PCA and GSVA (**f**)analyses based on risk score

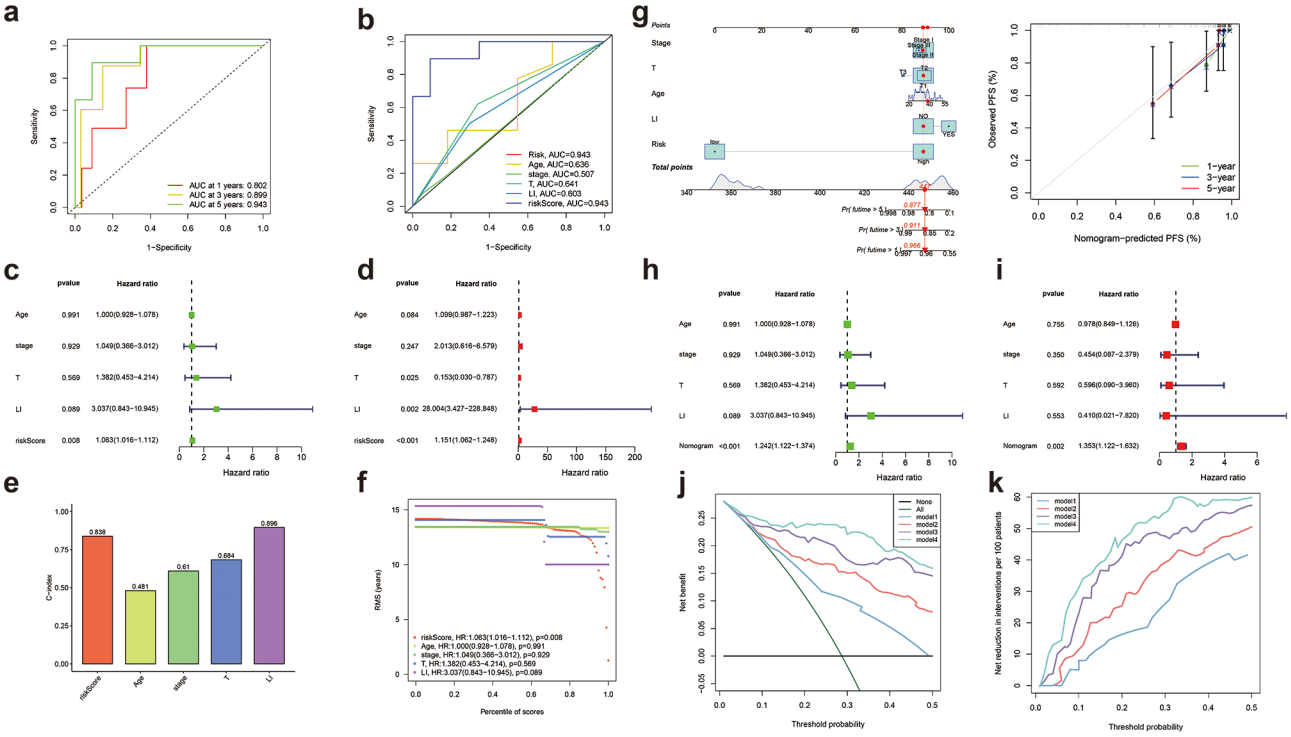

Fig. 4 The construction and validation of nomogram. (**a**) ROC analysis of risk score on PFS at 1-, 3-, and 5-years follow up in TCGA seminoma cohort. (**b**) The time-dependent ROC curves for risk, age, stage, T, lymphovascular invasion (LI), and risk score at 5-years follow up. Forrest plot of univariate (**c**) and multivariate (**d**) Cox regression analysis of age, stage, T, LI, and risk score. (**e**) The C-index and restricted mean survival (RMS) analysis (**f**) of risk score, age, stage, T and LI. (**g**) The nomogram and calibration plots to predict 1-, 3-, and 5-year PFS. Forrest plot of univariate (**h**) and multivariate (**i**) Cox regression analysis of age, stage, T, LI, and nomogram. (**j-k**) The DCA analysis of 4 models. (model 1: age, stage, T, LI, and serum markers; model 2: the expression of CTLA4, TMX1, and SNX17, risk score, nomogram; model 3: T, LI, risk score, nomogram, and serum markers; model 4: LI and risk score)

on multivariable Cox regression analysis. The C-index ranges from 0 to 1, where 1 indicates perfect discrimination and 0.5 implies random chance. The C-index of the risk score was 0.838, lower than that of LI (0.896) but higher than that of the other factors. Only the risk score factor was identified as a risk factor for determining the prognosis of seminoma patients based on restricted mean survival (RMS) analysis, with a p value of 0.008, HR of 1.063, and 95% CI of 1.016–1.112 (Fig. 4f).

We established an accurate and stable hybrid nomogram comprising clinic-pathological characteristics (age, stage, T, LI), and the novel IRPS (Fig. 4g). To utilize the nomogram, individual patients' specific points (black dots) are positioned on each variable axis. Red lines and dots ascend to determine points assigned to each variable; their cumulative sum (447) is positioned on the Total Points axis. Then, a line descends to the survival axes, computing the probability of 5-year (87.7%), 3-year (91.1%), and 1-year (96.6%) progression-free survival. Within this integrated nomogram, the risk score model demonstrated significant influence among these clinically relevant covariates, consistent with findings from RMS and multivariable Cox regression analysis. Consequently, the IRPS could aid in clinical management for predicting relapse among seminoma patients. The calibration curve for the PFS nomogram showed excellent agreement between prediction and observation. Subsequently, univariable and multivariable Cox regression analyses were performed to evaluate the nomogram. Notably, upon integrating the nomogram with confounding factors, LI ceased to be a risk factor, while the nomogram remained significant (Fig. 4h and i).

The decision curve plots the sensitivity and specificity of the predictive model on the horizontal axis against net benefits on the vertical axis. A reference strategy with a benefit of 0 ensures that its decision curve consistently lies below the x-axis. In decision curve analysis (DCA), the closer the predictive model's decision curve aligns with that of the reference strategy, the less practical the predictive model becomes clinically. In this study, four models were constructed and evaluated using DCA to assess their predictive capabilities. Model 1 included age, stage, T, LI, and serum markers (LDH, HCG, and AFP); Model 2 comprised CTLA4 expression, TMX1 expression, SNX17 expression, risk score, and nomogram; Model 3 integrated T, LI, risk score, nomogram, and serum markers; and Model 4 involved LI, risk score. Model 4 exhibited superior net benefits compared to the

other three models (Fig. 4j). Additionally, the highest reduction in net interventions was observed in Model 4 (Fig. 4k).

Immune landscape exploration

CIBERSORT analysis was employed to assess the immune infiltration disparity between high and low-risk groups. As depicted in Fig. 5a, there were notable distinctions in the infiltration of naïve B cells, memory B cells, and gamma delta T cells. Moreover, the distinct infiltration pattern of B cells may be associated with TMX1 and SNX17 expressions (Fig. 5c). Elevated TMX1 and SNX17 expression correlated with a decreased fraction of memory B cells and an increased fraction of naïve B cells, ultimately resulting in PFS time (Fig. 5d and e). Furthermore, increased CTLA4 expression was linked to a higher fraction of T cells gamma delta and improved PFS (Fig. 5f).

The disparities in immune function between high and low-risk groups were also examined (Fig. 5b). Notably, immune functions related to APC co-inhibition, APC co-stimulation, CCR, checkpoint regulation, cytolytic activity, HLA, inflammation promoting, parainflammation, T cell co-inhibition, and T cell co-stimulation were all significantly suppressed in the high-risk group. Furthermore, patients in the high-risk group exhibited lower TIDE (Fig. 5g) and dysfunction scores (Fig. 5h), along with higher exclusion (Fig. 5i). High-risk group patients had a higher proportion of patients predicted to respond to immunotherapy ($p<0.01$, Fig. 5j).

In this study, we designated testicular tumor homogenate as control cells and renal hilus lymph node homogenate as treated cells for single-cell RNA sequencing (scRNA-seq) analysis. Our findings indicate that CTLA4 is predominantly expressed in T cells (Fig. 5k. 5 L). Moreover, a diminished distribution of T cells was observed in renal hilus lymph node tissues (Table S3, $P<0.001$, avg_log2FC=7.99). Notably, TMX1 exhibited significant expression in smooth muscle cells, monocytes, and macrophages. In comparison to the testicular tumor homogenate, TMX1 demonstrated upregulation in smooth muscle cells and macrophages within the renal hilus lymph node homogenate. Furthermore, SNX17 showed significant expression in NK cells, B cells, and macrophages, with upregulation observed in these cells compared to the control cells derived from testicular tumors.

Molecular screening, docking, and simulating

The potential molecular which may upregulate CTLA4, downregulate TMX1 and SNX17 were obtained from the Pubchem database. After docking with the molecular database respectively, ICG-001, Rutin, and Doxorubicin displayed the lowest combining energy (ΔGMMGBSA=-30.48, -27.39, -17.23 KCal/Mol) and most connecting bonds with the corresponding protein complex. The Free Energy Landscape provides insight into the interactions and energy distribution among molecules within the system, facilitating comprehension of interaction characteristics, conformational states, and stability. This information proves invaluable in designing molecular interaction mechanisms and materials. The landscape, in this instance, is delineated by two key indicators: RMSD (Root Mean Square Deviation) and R(g) (Radius of Gyration). Throughout the simulation, we identified low-energy regions indicative of molecules adopting various interaction modes or conformations to attain minimum energy states.

Root Mean Square Deviation (RMSD) serves as a metric for assessing alterations in protein structure. In this simulation, we computed the RMSD values between proteins and small molecules and visualized the RMSD trends (Fig. 6a and c). Our findings revealed that within the initial 100 nanoseconds of the three simulations, the RMSD values between proteins and small molecules exhibited considerable variability before stabilizing gradually. Throughout the simulation, the RMSD values consistently remained within a narrow range, suggesting a stable binding between proteins and small molecules.

Gyrate serves as an indicator to assess the overall compactness of proteins. In this simulation, Gyrate were computed between proteins and small molecules (Fig. 6d). Our analysis revealed that following the binding with small molecules, the Gyrate of the protein decreased compared to individual protein molecules, suggesting that the binding of small molecules leads to increased compactness of the protein molecules.

To ascertain the reasonableness of the binding between proteins and small molecules, several additional indicators warrant evaluation. The rationality of their interaction can be further elucidated through analyses such as distance distribution function and hydrogen bonding assessment (Figure S3a) within the simulation. Based on these findings, it can be inferred that the interaction between proteins and small molecules is stable. Moreover, the binding of small molecules induces compaction in protein molecules, reduces surface area (Figure S3b), and fosters the formation of numerous hydrogen bonds with the small molecules. RMSF serves as an indicator for assessing protein dynamics. In this simulation, we calculated the RMSF values for proteins and small molecules, subsequently plotting the RMSF chart (Figure S3c). The results indicated that the RMSF value of the protein was lower in the binding region and higher in the non-binding region, suggesting that small molecule binding influences the stability of the protein.

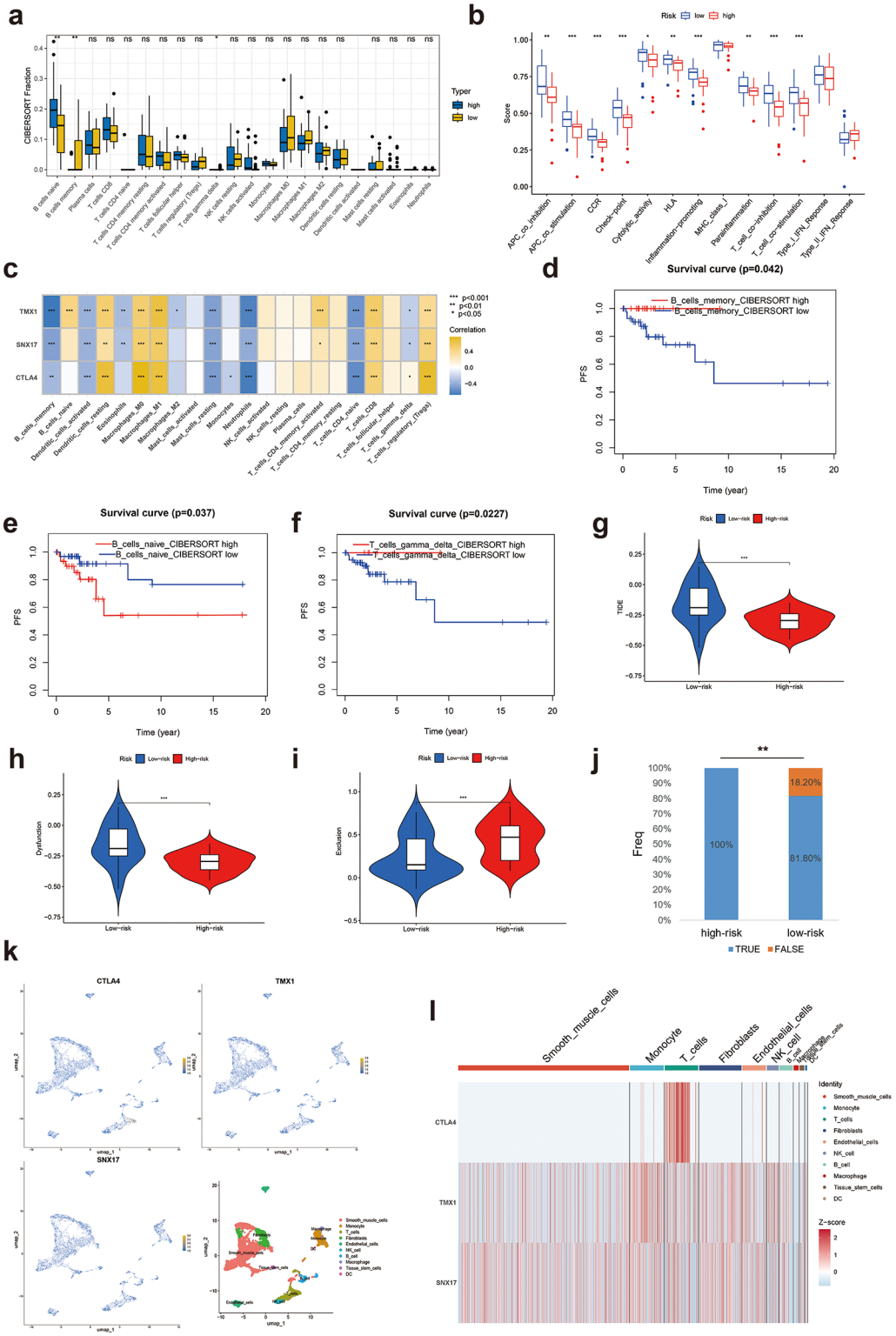

Fig. 5 The immune landscape and immunotherapy efficacy validation based on risk group. (**a**) The cibersort infiltration of 22 tumor immune cells in high- and low-risk group patients. (**b**) The immune function differences between high- and low- risk groups. (**c**) The correlation between the expression of 3 IRSGS and infiltration of 22 immune cells. (**d-f**) The survival curves of PFS related immune cells. The difference of TIDE (**g**), dysfunction (**h**), exclusion (**i**), and potential immunotherapy responders (**j**) between high- and low-risk groups. (**k**) The expression distribution and abundance of the 3 IRSGs based on the sing-cell RNA sequencing (GSE197778). (**l**) The expression heat map of the 3 IRSGs in seminoma tissues

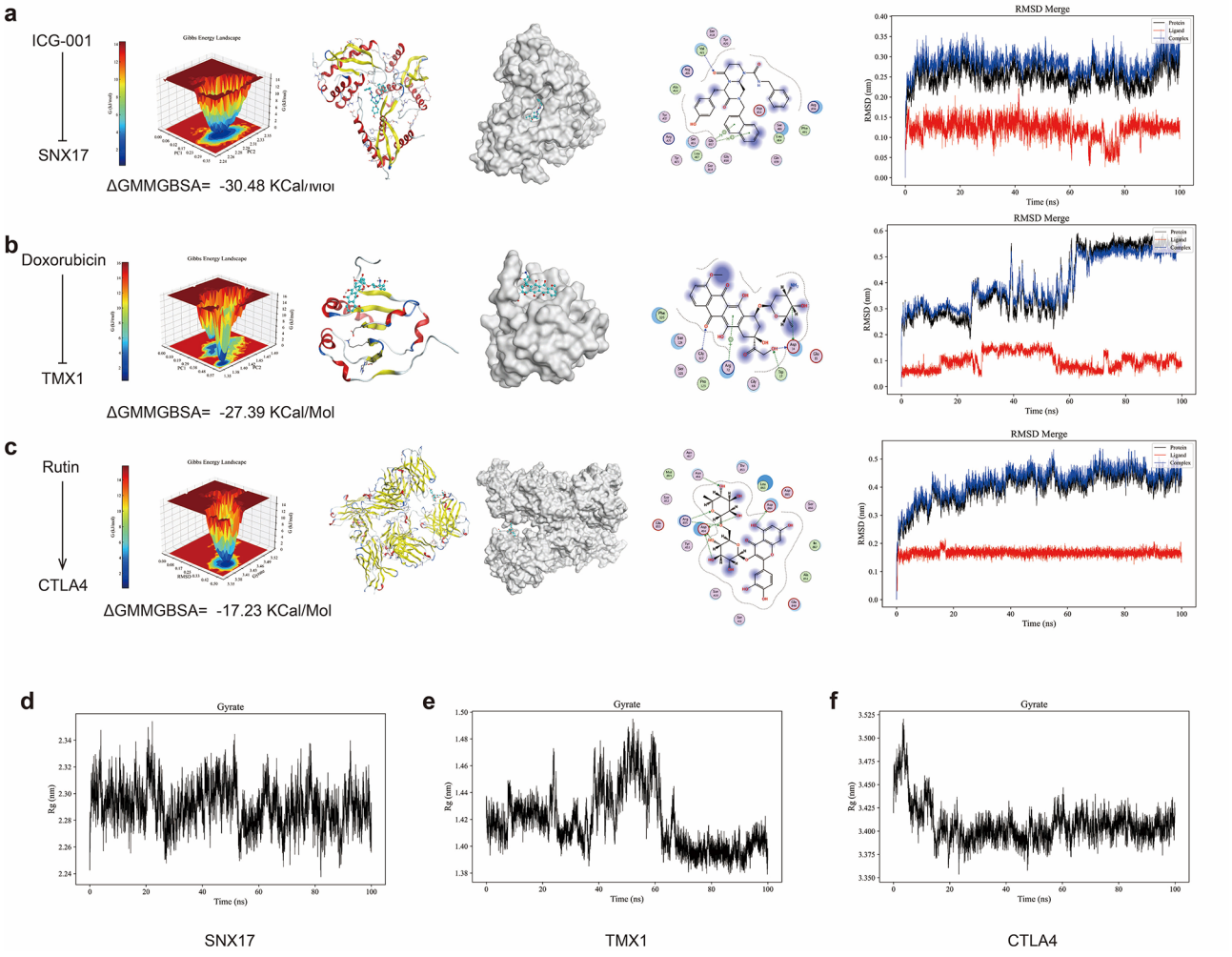

Fig. 6 The molecular docking and dynamics simulation of 3 pairs of molecular-protein complex. (**a**) Free energy landscape and molecular docking of the binding simulation between molecular component ICG-001 and protein SNX17, Doxorubicin and TMX1 (**b**), Rutin and CTLA4 (**c**). (**d-f**) The Gyrate charts of the three complexes

Rutin, ICG-001, and Doxorubicin could suppress the proliferation and invasion ability of Tcam-2 cells in vitro and vivo assays

To evaluate distinctions in the expression patterns of IRSGs and the infiltration patterns of immune cells between relapse and non-relapse seminoma tissues, IF assays were conducted (Fig. 7). Notably, an elevated expression of CTLA4 was observed in non-relapse seminoma tissues, concomitant with an increased fluorescence signal of CD3, a marker for gamma delta T cells. Conversely, TMX1 and SNX17 exhibited upregulation in relapse seminoma tissues, coinciding with a decrease in the infiltration of memory B cells (CD27). Moreover, the infiltration of naïve B cells (CD22) mirrored the expression pattern of TMX1. Additionally, the upregulation of Vimentin, an indicator of cell invasion viability, was noted in relapse patients, suggesting heightened invasion and metastatic potential, indicative of a higher recurrence rate. These findings are consistent with those depicted in Fig. 5c and f.

At concentrations of 38.19 μM for Rutin, 10.96 μM for ICG-001, and 0.3994 μM for Doxorubicin, the IC50 values were determined for the treatment of Tcam-2 cells. This resulted in significant inhibition of cell proliferation, with the most pronounced differences observed at 2 days, 4 days, and 3 days, respectively, compared to the control DMSO group (Fig. 8a). Following treatment with Rutin, both mRNA and protein expression levels of CTLA4 were upregulated. Conversely, treatment with Doxorubicin and ICG-001 resulted in the downregulation of mRNA and protein expression levels of TMX1 and SNX17, respectively. With the application of the three molecular treatments, the colony numbers of Tcam-2 cells exhibited a reduction (Fig. 8b).

To investigate the impact of three molecular compounds on the metastatic potential of Tcam-2 cells, we performed wound healing and transwell assays. The cells

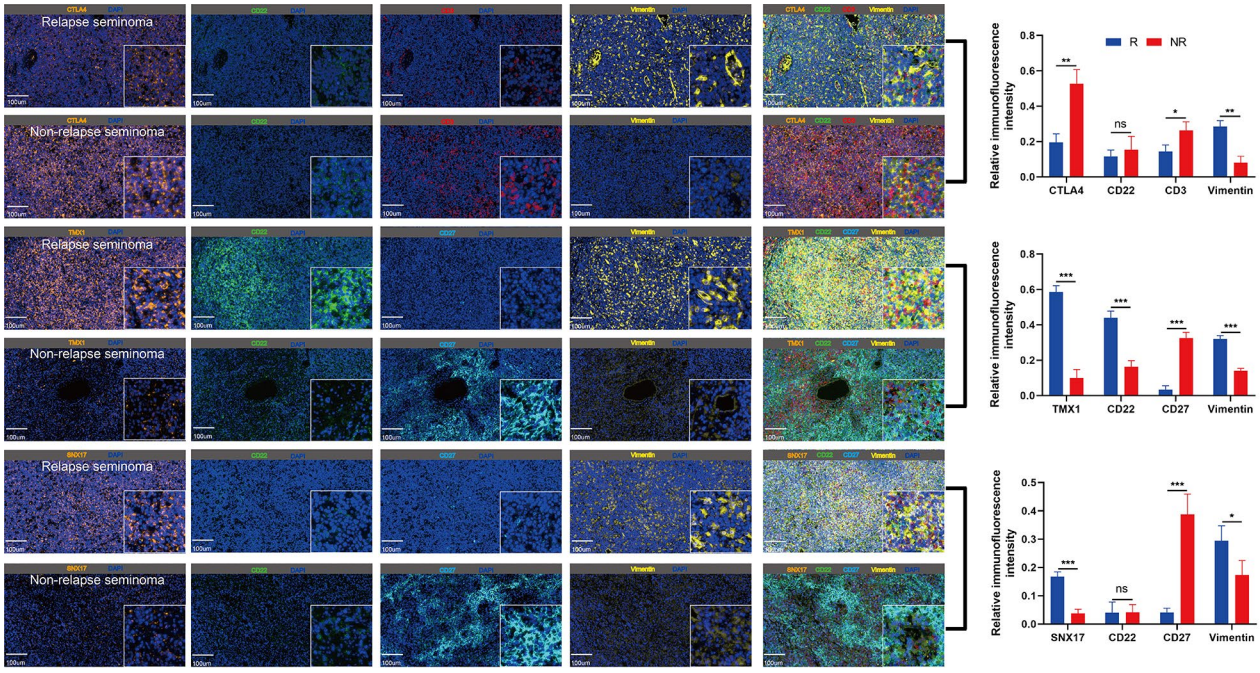

Fig. 7 The IF staining of relapse and non-relapse seminoma samples in the 3 IRGs (orange), CD22 (green), CD3 (red), CD27 (aqua), vimentin (yellow)

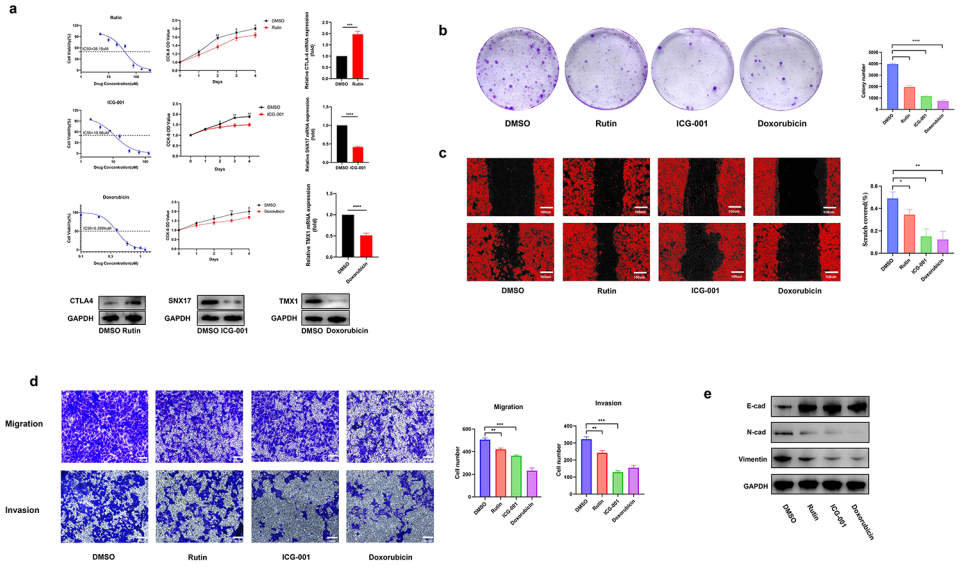

Fig. 8 The in vitro study. (**a**) The mRNA and protein expression difference after treated with correspond molecular component at IC50 effective concentration. The colony formation (**b**), wound healing (**c**), and transwell assays (**d**) with Tcam-2 cells treated with molecular components. (**e**) The protein expression of Epithelial-Mesenchymal Transition (EMT) markers (E-cad, N-cad, Vimentin) in Tcam-2 cells treated with molecular components

treated with these compounds exhibited reduced wound healing capacity compared to the control group, particularly evident with Doxorubicin (Fig. 8c). Notably, Rutin, ICG-001, and Doxorubicin significantly hindered the migration and invasion abilities of Tcam-2 cells (Fig. 8d). This effect coincided with an elevation in E-cadherin expression levels and a decrease in the expression levels of vimentin and N-cadherin (Fig. 8e).

The testicular xenograft in situ was conducted to validate findings from in vitro assays. Photographs and H&E staining of the testicular xenografts are presented in Fig. 9a. Tumor cells predominantly infiltrated the interstitial tissue. The tumor masses were excised from the testis (Fig. 9b) and assessed for weight and volume. Compared to the DMSO group, the Rutin, ICG-001, and Doxorubicin treatment groups exhibited smaller tumor masses in both weight and volume. Subsequently, the tumor masses

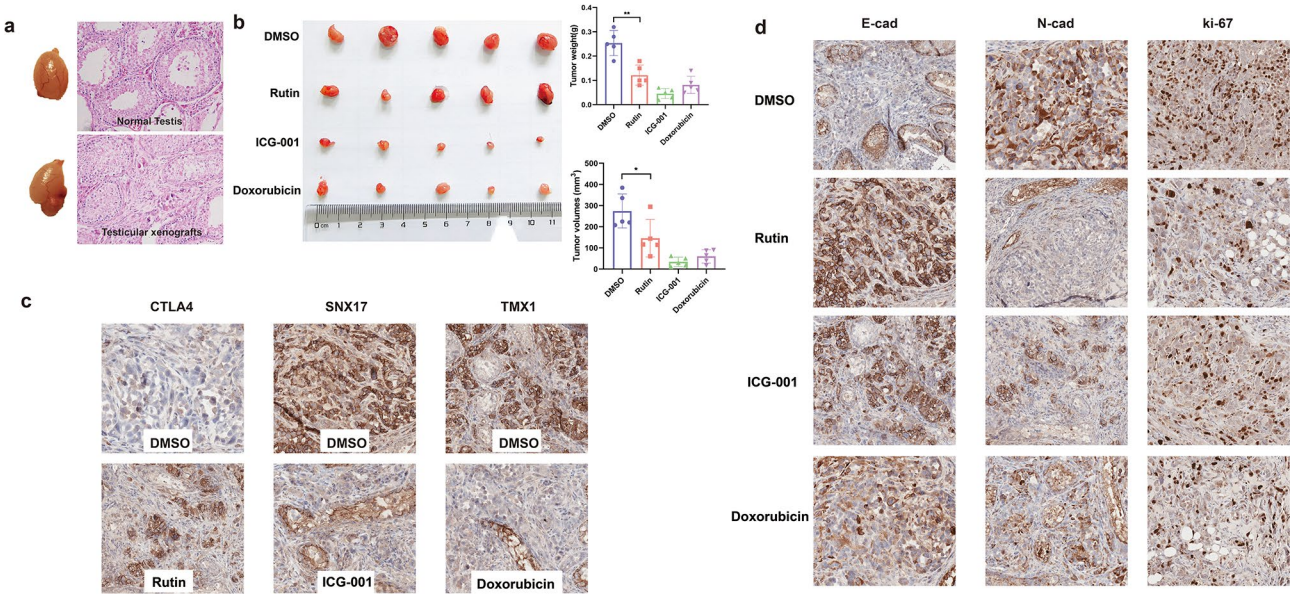

Fig. 9 The in vivo study. (**a**) Photographs and H&E staining of the testicular xenografts in situ. (**b**) The tumor masses isolated from testes were measured with weight and volume. (**c**) The tumor masses were stained with CTLA-4, SNX17 and TMX1. (**d**) The tumor masses were stained with E-cad, N-cad, and ki-67

were stained for CTLA-4, SNX17, and TMX1 (Fig. 9c). Treatment with Rutin resulted in upregulated CTLA-4 protein expression in the tumor masses. Conversely, treatment with ICG-001 and Doxorubicin downregulated the expression of SNX17 and TMX1, respectively. Furthermore, treatment with these three molecular compounds upregulated E-cad expression and downregulated N-cad and Ki-67 expression, indicating inhibition of proliferation and invasion abilities (Fig. 9d).

Discussion

Testicular germ cell tumor (TGCT) exhibits high sensitivity to cisplatin-based chemotherapy, and the integration of surgery and radiation therapy in carefully selected cases has resulted in a high cure rate for this disease. Nevertheless, patients experiencing disease progression following surgery often display a low response to chemotherapy. Therefore, it is essential to elucidate the underlying molecular mechanisms and prognostic markers linked to unfavorable outcomes within this particular patient subset. To date, a validated immune-related signature capable of predicting response to immunotherapy and PFS remains elusive. This highlights the necessity to identify a prognostic biomarker specifically tailored for immunotherapy in seminoma.

Cytokine related pathways were frequently enriched in this study, including "Cytokine-mediated signaling pathway" in GO analysis and "Cytokine-cytokine receptor interaction" pathway in KEGG and GSVA analysis based on keycluster genes and risk score respectively. We have reported that cytokine related pathways were significantly correlate to the invasion and metastasis of seminoma cells [14]. High expression levels of cytokines CCR5 and CXCR4 were associated with poor prognosis for seminoma patients [15].

The post-testicular resection treatment plan encompasses active monitoring, maintenance therapy for relapsed patients, or risk-adaptive treatment, coupled with monitoring for low recurrence risk patients, and administering cisplatin-based adjuvant chemotherapy for high recurrence risk patients. Nevertheless, consensus remains elusive regarding the definition of high recurrence risk and the utilization of risk factors for patient classification. While Warde et al.'s publication introduced tumor size (>4 cm) and testicular reticulum invasion as criteria for identifying patients at high risk of recurrence in clinical guidelines [16], the evidential support for these risk factors in clinical decision-making is notably scant. The correlation between testicular reticulum invasion and heightened recurrence risk lacks consistency, leaving uncertainty about its independence as a predictor of recurrence. Although numerous studies underscore the prognostic relevance of tumor size [17, 18], the evidence substantiating the 4 cm threshold for risk stratification remains ambiguous, and reliance solely on tumor size for risk stratification fails to establish its clinical utility definitively. A systematic review revealed that the 5-year recurrence risk for tumors > 4 cm and ≤ 4 cm ranged from 17.4 to 27.0% and 4.5–13.4%, respectively [19]. In high-risk scenarios (tumors ≥ 6 cm), the 10-year cumulative risk of recurrence reaches 32.0%, suggesting that adjuvant therapy based on tumor size risk assessment may result

in overtreatment for approximately two-thirds of patients [20]. The DCA curves estimated by our nomogram indicates that the inclusion of LI and risk score, (Model 4) in predicting PFS in patients with adnexal masses offers a net benefit over the strategies of treating all or none, thereby aiding clinicians and patients in decision-making regarding chemotherapy administration.

Through a series of analysis and screening, CTLA4, TMX1, and SNX17 were adopted to construct the IRPS, of which CTLA4 was defined as protective factor, SNX17 and TMX1 were considered as risk factors. CTLA4 is often known as the accomplice of tumor cells, which could be activated by tumor cells, deactivate activated T cells, thereby achieving immune escape of the tumor itself. CTLA-4 blockers, including Tremelimumab, Ipilimumab and so on, aim to induce anti-tumor immune responses by promoting the activation and proliferation of tumor specific T cells, which have been broadly applied in various malignant tumors, such as lung cancer, esophageal cancer, etc. On the contrary, for advanced seminoma patients, CTLA4 may play as a guardian role. In a previous study, CTLA-4 positivity in immune cells did not associate with clinicopathological variables of testicular cancer. However, patients with CTLA-4 immunoexpression in immune cells above the 50% cutoff exhibited significantly less LI and presented with lower pT stage and N stage when compared to those with < 50% positive immune cells [21]. We found that CTLA4 was downregulated in relapse seminoma tissues, which lead to lower fraction of T cells gamma delta and bad outcomes. Rutin (Pubchem ID: 5280805) is a rutinoside that is quercetin with the hydroxy group at position C-3 substituted with glucose and rhamnose sugar groups. It has a role as a metabolite and an antioxidant [22]. Rutin has been reported to activate human immune cells for resisting tumor cells [23] and increase expression of CTLA4 mRNA [24]. We have used molecular docking and dynamics to demonstrate this, along with ICG-001 (Pubchem ID: 11238147) in decreasing SNX17 [25], Doxorubicin (Pubchem ID: 31703) in decreasing TMX1 [26].

In our investigation, we observed a positive correlation between the cell marker CD3 of gamma delta T cells and the expression of CTLA4, resulting in diminished levels of Vimentin expression and a higher recurrence rate. Furthermore, the infiltration level of naïve B cells displayed a positive association with TMX1, whereas the infiltration level of memory B cells showed a negative correlation with TMX1 and SNX17. Consequently, elevated expression levels of TMX1 and SNX17, coupled with increased infiltration of naïve B cells and decreased infiltration of memory B cells, were associated with a heightened recurrence rate among patients. Subsequent cell biology experiments revealed that three molecular compounds, identified through screening, docking, and simulation, significantly inhibited the proliferation, migration, and invasion capacities of Tcam-2 cells. Our research has several limitations: (1) The underlying mechanisms by which the three molecular compounds inhibit seminoma cell viability were not elucidated in this study. Future investigations will aim to explore the potential mechanisms of action of these compounds on testicular tumor cells. (2) The specific immune cells targeted by these three signature immune-related genes and their potential modes of action remain unclear. However, based on current CIBERSORT and immunofluorescence results, it is suggested that CTLA4 may regulate T cells, while TMX1 and SNX17 may influence B cells. (3) In the in vivo study, metastatic foci from the testicular xenograft in situ were not observed or collected. Analyzing these foci could enhance our understanding of the differences in tumor cell metastatic ability under the intervention of molecular compounds.

Conclusion

Our study initially developed an IRPS and validated its potential in predicting relapse among seminoma patients. Model 4, constructed through DCA, could assist clinicians and patients in determining whether chemotherapy is necessary. Patients classified as high-risk according to our signature might derive less benefit from traditional chemotherapy regimens but could potentially benefit more from ICI therapy. Additionally, we observed that the three molecular compounds targeting the signature genes could markedly suppress the proliferation and invasion of seminoma tumor cells.

Abbreviations

TGCTs	Testicular germ cell tumors
β-HCG	β-human chorionic gonadotropin
LDH	Lactate dehydrogenase
TCGA	The Cancer Genome Atlas
R	Relapse
NR	Non-relapse
GEO	The Gene Expression Omnibus
scRNA-seq	Single cell RNA-seq
GTEx	The Genotype-Tissue Expression
TOM	Topological overlap matrix
Mcode	Molecular Complex Detection
GSEA	Gene set enrichment analyses
GO	Gene Ontology
KEGG	Kyoto Encyclopedia of Genes and Genomes
IRPS	Immune-related Prognostic Signature
PFS	Progression free survival
AIC	Akaike information criterion
LI	Lymphovascular Invasion
IRGs	Immune related genes
IRSGs	Immune-related signature genes
C-index	Concordance index
DCA	Decision Curve Analysis
TIDE	Tumor immune dysfunction and exclusion
IHC	Immunohistochemistry
IF	Immunofluorescence

Supplementary Information

The online version contains supplementary material available at https://doi.org/10.1186/s12964-024-01927-w.

Supplementary Material 1: The correlation between the logarithm of node connectivity (log(k)) and the logarithm of node probability (log(P(k)))

Supplementary Material 2: Significantly mutated genes in the mutated seminoma samples of high- and low-risk groups.

Supplementary Material 3: (a)The hydrogen bond (HBond), (b) solvent accessible surface area charts (SASA) and root-mean-square fluctuation (RMSF) of the 3 pairs of molecular-protein complex.

Supplementary Material 4

Supplementary Material 5

Acknowledgements
We acknowledge all participants in this study.

Author contributions
Conceptualization, YC; Data curation, YC and JZ; Formal analysis, YC and XZ; Investigation, BF and JG; Methodology, YC and BL; Project administration, YC and FX; Software, YC and HT; Validation, HH and BL; Visualization, YC and FX; Writing – original draft, YC; Writing – review & editing, FX and XS. All authors read and approved the final manuscript.

Funding
This study was supported by the National Nature Science Foundation of China (NO. 81972402); The subject of Nanjing Jinling Hospital (YYMS2021025;2023JCYJYB112).

Data availability
Data is provided within the manuscript or supplementary information files.

Declarations

Ethics approval and consent to participate
This study was approved by the medical ethics committee of The Jinling Hospital (DZGZRDW240021; 2024DZGJJ-021) and conducted in accordance with the Declaration of Helsinki. All patients included in this study provided informed consent.

Consent for publication
Not applicable.

Competing interests
The authors declare no competing interests.

Author details
[1]Department of Urology, Jinling Hospital, Affiliated Hospital of Medical School, Nanjing University, Nanjing, China
[2]Department of Pathology, Jinling Hospital, Affiliated Hospital of Medical School, Nanjing University, Nanjing, China
[3]Jiangsu Product Quality Testing & Inspection Institute, Nanjing, China
[4]Department of Urology, The First Afliated Hospital of Nanjing Medical University, Nanjing, China

Received: 28 August 2024 / Accepted: 4 November 2024
Published online: 21 November 2024

References

1. Cedeno JD, Light DE, Leslie SW, Testicular Seminoma. *StatPearls*. StatPearls Publishing Copyright © 2024, StatPearls Publishing LLC.; 2024.
2. Cheng L, Albers P, Berney DM, et al. Testicular cancer. Nat Rev Dis Primers Oct. 2018;5(1):29. https://doi.org/10.1038/s41572-018-0029-0.
3. Siegel RL, Miller KD, Wagle NS, Jemal A. Cancer statistics, 2023. CA Cancer J Clin Jan. 2023;73(1):17–48. https://doi.org/10.3322/caac.21763.
4. Kier MG, Lauritsen J, Mortensen MS, et al. Prognostic factors and treatment results after bleomycin, Etoposide, and cisplatin in germ cell Cancer: a Population-based study. Eur Urol Feb. 2017;71(2):290–8. https://doi.org/10.1016/j.eururo.2016.09.015.
5. Mortensen MS, Lauritsen J, Gundgaard MG, et al. A nationwide cohort study of stage I seminoma patients followed on a surveillance program. Eur Urol Dec. 2014;66(6):1172–8. https://doi.org/10.1016/j.eururo.2014.07.001.
6. Warde P, Specht L, Horwich A, et al. Prognostic factors for relapse in stage I seminoma managed by surveillance: a pooled analysis. J Clin Oncol Nov. 2002;15(22):4448–52. https://doi.org/10.1200/jco.2002.01.038.
7. Wagner T, Toft BG, Lauritsen J, et al. Prognostic factors for relapse in patients with clinical stage I testicular seminoma: a Nationwide, Population-based Cohort Study. J Clin Oncol Jan. 2024;1(1):81–9. https://doi.org/10.1200/jco.23.00959.
8. Bagrodia A, Lee BH, Lee W, et al. Genetic determinants of Cisplatin Resistance in patients with Advanced Germ Cell tumors. J Clin Oncol Nov. 2016;20(33):4000–7. https://doi.org/10.1200/jco.2016.68.7798.
9. Alsaab HO, Sau S, Alzhrani R, et al. PD-1 and PD-L1 Checkpoint Signaling Inhibition for Cancer Immunotherapy: mechanism, combinations, and clinical outcome. Front Pharmacol. 2017;8:561. https://doi.org/10.3389/fphar.2017.00561.
10. Wolchok JD, Chiarion-Sileni V, Gonzalez R, et al. Long-term outcomes with Nivolumab Plus Ipilimumab or Nivolumab alone Versus Ipilimumab in patients with Advanced Melanoma. J Clin Oncol Jan. 2022;10(2):127–37. https://doi.org/10.1200/jco.21.02229.
11. Chovanec M, Cierna Z, Miskovska V, et al. Prognostic role of programmed-death ligand 1 (PD-L1) expressing tumor infiltrating lymphocytes in testicular germ cell tumors. Oncotarget Mar. 2017;28(13):21794–805. https://doi.org/10.18632/oncotarget.15585.
12. Cierna Z, Mego M, Miskovska V, et al. Prognostic value of programmed-death-1 receptor (PD-1) and its ligand 1 (PD-L1) in testicular germ cell tumors. Ann Oncol Feb. 2016;27(2):300–5. https://doi.org/10.1093/annonc/mdv574.
13. Van Der Spoel D, Lindahl E, Hess B, Groenhof G, Mark AE, Berendsen HJ. GROMACS: fast, flexible, and free. J Comput Chem Dec. 2005;26(16):1701–18. https://doi.org/10.1002/jcc.20291.
14. Cui Y, Miao C, Liu S, et al. Clusterin suppresses invasion and metastasis of testicular seminoma by upregulating COL15a1. Mol Ther Nucleic Acids Dec. 2021;3:26:1336–50. https://doi.org/10.1016/j.omtn.2021.11.004.
15. Chen YH, Lin TT, Wu YP, et al. Identification of key genes and pathways in seminoma by bioinformatics analysis. Onco Targets Ther. 2019;12:3683–93. https://doi.org/10.2147/ott.S199115.
16. Chung P, Warde P. Stage I seminoma: adjuvant treatment is effective but is it necessary? J Natl Cancer Inst Feb. 2011;2(3):194–6. https://doi.org/10.1093/jnci/djq535.
17. Boormans JL, Sylvester R, Anson-Cartwright L, et al. Prognostic factor risk groups for clinical stage I Seminoma: an Individual Patient Data Analysis by the European Association of Urology Testicular Cancer Guidelines Panel and Guidelines Office. Eur Urol Oncol Jun. 2024;7(3):537–43. https://doi.org/10.1016/j.euo.2023.10.014.
18. Huang W, Luo J, Zhou X, Zhao Y, Zhang T, Ma X. Nomograms for Predicting Prognosis of primary Mediastinal Seminoma: a Population-based study. J Oncol. 2021;2021:9048375. https://doi.org/10.1155/2021/9048375.
19. Boormans JL, Mayor de Castro J, Marconi L, et al. Testicular tumour size and Rete Testis Invasion as prognostic factors for the risk of Relapse of Clinical Stage I Seminoma Testis patients under Surveillance: a systematic review by the Testicular Cancer guidelines Panel. Eur Urol Mar. 2018;73(3):394–405. https://doi.org/10.1016/j.eururo.2017.09.025.
20. Mortensen MS, Bandak M, Kier MG, et al. Surveillance versus adjuvant radiotherapy for patients with high-risk stage I seminoma. Cancer Apr. 2017;1(7):1212–8. https://doi.org/10.1002/cncr.30458.
21. Lobo J, Rodrigues Â, Guimarães R, et al. Detailed characterization of Immune Cell infiltrate and expression of Immune Checkpoint molecules PD-L1/CTLA-4 and MMR Proteins in testicular germ cell tumors disclose Novel Disease biomarkers. *Cancers (Basel)*. Oct. 2019;11(10). https://doi.org/10.3390/cancers11101535.
22. Pan RY, Ma J, Kong XX, et al. Sodium rutin ameliorates Alzheimer's disease-like pathology by enhancing microglial amyloid-β clearance. Sci Adv Feb. 2019;5(2):eaau6328. https://doi.org/10.1126/sciadv.aau6328.
23. Singh S, Kumar K, Panda M, Srivastava A, Mishra A, Prajapati VK. High-throughput virtual screening of small-molecule inhibitors targeting immune cell

checkpoints to discover new immunotherapeutics for human diseases. Mol Divers Apr. 2023;27(2):729–51. https://doi.org/10.1007/s11030-022-10452-2.
24. Luceri C, Giovannelli L, Pitozzi V, et al. Liver and colon DNA oxidative damage and gene expression profiles of rats fed Arabidopsis thaliana mutant seeds containing contrasted flavonoids. Food Chem Toxicol Apr. 2008;46(4):1213–20. https://doi.org/10.1016/j.fct.2007.10.007.
25. Gaddis M, Gerrard D, Frietze S, Farnham PJ. Altering cancer transcriptomes using epigenomic inhibitors. Epigenetics Chromatin. 2015;8:9. https://doi.org/10.1186/1756-8935-8-9.
26. Verheijen M, Schrooders Y, Gmuender H, et al. Bringing in vitro analysis closer to in vivo: studying doxorubicin toxicity and associated mechanisms in 3D human microtissues with PBPK-based dose modelling. Toxicol Lett Sep. 2018;15:294:184–92. https://doi.org/10.1016/j.toxlet.2018.05.029.

Publisher's note